Supplementary Material for "Direct observation of phosphate inhibiting the force-generating capacity of a mini-ensemble of myosin molecules"

E. P. Debold, S. Walcott, M. Woodward and M. A. Turner

1 Laser trap data analysis

Binding events were determined using a threshold-crossing routine based on a deviation from the signal baseline using commercially available software program (Clamp FitTM v10.2). The baseline value was determined from a section of data in which the bead-actin-bead assembly (Fig. 2 Main text) was held away from the pedestal and thus not capable of interacting with myosin. Displacements that exceeded the threshold value for $>$ 10ms were considered binding events (Fig. 1). Peak force of each event was determined based on the highest force achieved for at least 10ms (Fig. 1, expanded section). 10ms was chosen based on the estimated lifetime of the strongly bound state at the 100μM ATP concentration in the buffer from previous observations [1]. This reduced the probability of incorporating noise in the event population.

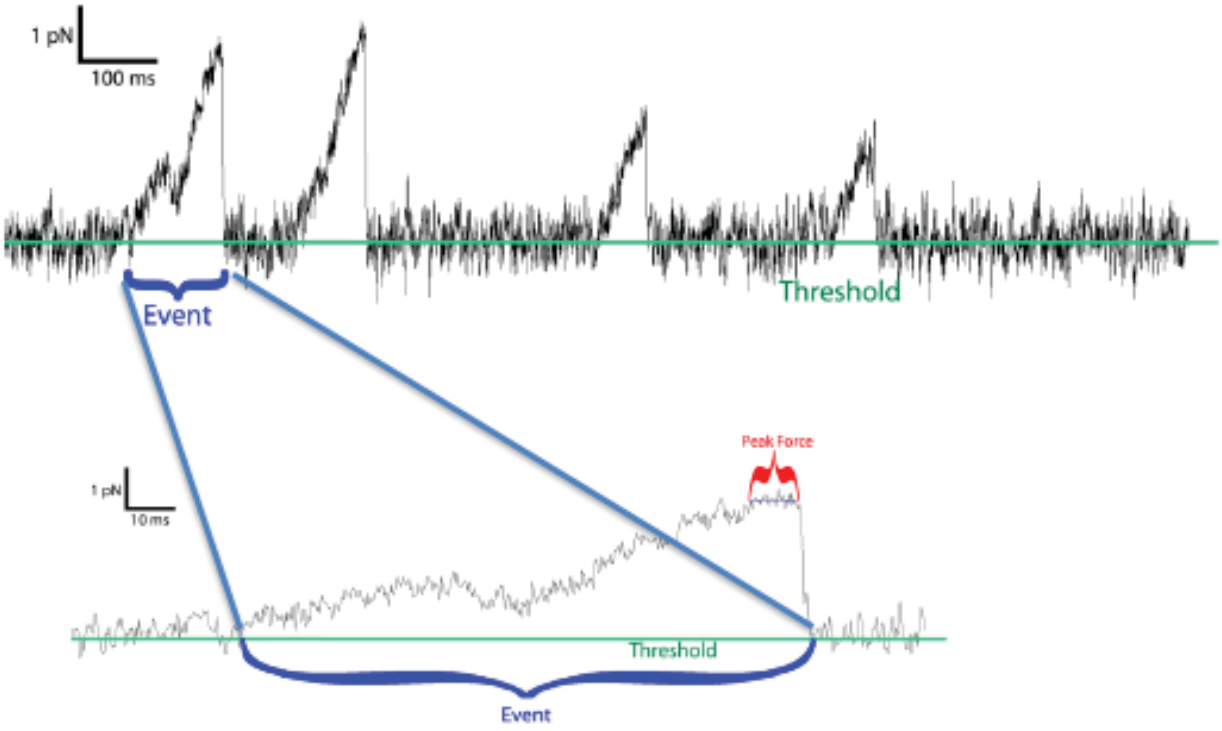

Figure 1: Demonstrating data analysis for measurements of small myosin ensembles in the laser trap. The top trace shows bead position as a function of time. Displacements are caused by myosin interactions. Inset (below) shows a sample "event" as well as the peak force (calculated from the known stiffness of the laser trap times the measured displacement).

Requiring a deviation from baseline eliminated the ability to detect zero displacement binding events that others have seen using variance thresholds [3] and Mean-Variance analysis (MV) [2], therefore we also performed a MV analysis on a subset of the 30mM P_i data (Fig. 2), which revealed a population of events with zero displacement, but the binding event population (e) was dominated by positive displacements, leading to a step size estimate (14nm) very similar to the value from the threshold crossing method (13nm). Choosing 10ms as the minimum event lifetime also likely resulted in an overestimate of the event lifetime. This overestimation is evident from the difference in event duration calculated from the thresholding method (18±1 ms) and the MV analysis (14±1 ms). However, since differences between 0 and 5, 10 and 30mM Pi were large (Fig 2, Main text), this overestimation has little effect on our overall conclusions. Additionally, since we used the threshold crossing algorithm in our simulations (see "Running the model"), this overestimation does not affect our use of the model to interpret our measurements.

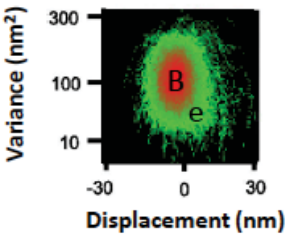

Figure 2: Mean variance analysis of measurements of small myosin ensembles in the laser trap. These data were collected at 30 mM P_i.

To further examine how our choice of threshold affected our measurements, we used the model to simulate experiments at 0 mM and at 30mM P_i and examined a threshold of 5, 10 and 20 ms. As expected, as we increase the threshold we no longer detect short events, and average event lifetime therefore increases (see Fig. 3A). Further, also as expected, since the short events have a relatively larger effect for the 30 mM P_i measurements, the relative difference in event lifetime between 0 and 30 mM P_i decreases with increasing threshold (see Fig. 3B). This analysis supports our claim that our choice of threshold does not effect our overall conclusions – namely that phosphate has a strong inhibitory effect on the actin binding of mini myosin ensembles.

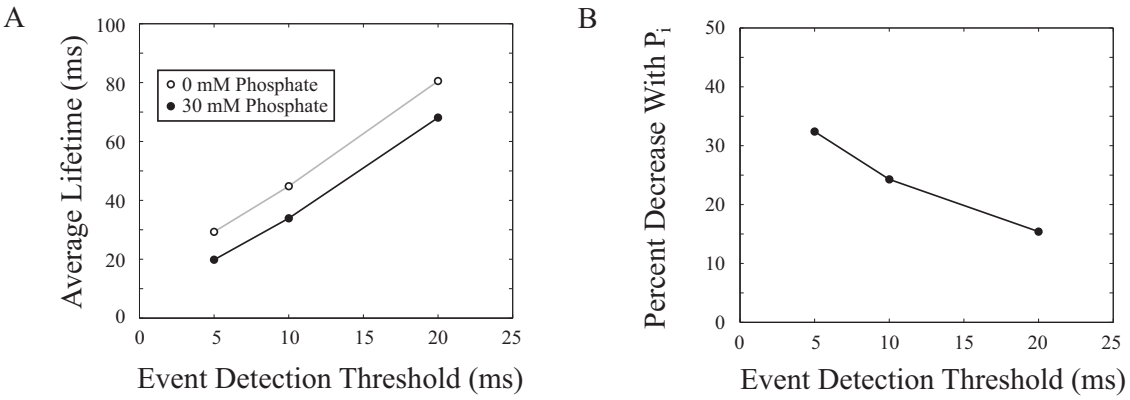

Figure 3: Our choice of threshold does not affect our conclusions. In our analysis, we used a 10 ms threshold for event detection. We performed simulations with our model to determine the effect of different choices of threshold. A. Shows average event lifetime as a function of event threshold in the presence and absence of 30 mM P_i. At all choices of threshold, phosphate causes event lifetime to decrease. B. Shows the relative decrease in average event lifetime upon the addition of 30 mM phosphate. The figure shows that a longer threshold tends to mask the inhibitory effect of phosphate. However, the 10 ms threshold is sufficient to resolve this inhibition.

1.1 Accounting for the non-linear range of the QPD

We used a quadrant photodiode (QPD) to detect bead position in the laser trap. This signal serves as the basis for all of our measurements. For small displacements (less than $\sim$ 250nm) the output of the QPD is proportional to bead position. For larger displacements, the output becomes non-linear. When we convert this signal to a force, we assume that the signal is linear. In the absence of phosphate, we occasionally observed displacements that approached the limit of this linear range. We therefore slightly underestimate the force for high force events.

To quantify this effect, we calibrated the trap by repeatedly displacing a bead a set distance (50 nm) and measuring the resulting QPD output. Without accounting for the non-linearity of the signal, we overestimate the displacement (and therefore the force, see Fig. 4A). For our measurements, this effect is quite small. For our data collected at a myosin density of 25 μg/mL, no events were outside the linear region (see Fig. 4B). For our data collected at a myosin density of 40 μg/mL, there were events outside the linear region (see Fig. 4B). The largest, which we measured at 7.04 pN without accounting for the non-linearity, becomes 8.25 pN when we correct for it. This error of around 15% for two out of the 433 events we collected under these conditions has a negligible effect on our results.

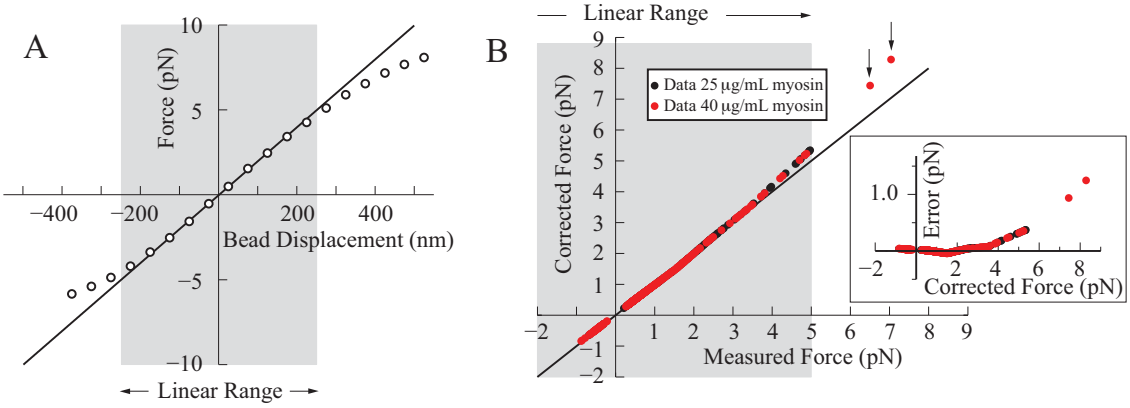

Figure 4: Correcting for non-linearities in the QPD signal. A. The QPD signal, converted to a putative force, as a function of bead displacement. We are able to very accurately measure force up to 5 pN. Above this value, we begin to underestimate force. B. The corrected force, that accounts for the non-linearity of the QPD as a function of the uncorrected force for all data collected in the absence of phosphate. Only two events (indicated with arrows) are outside the linear range and the effect is small, we underestimate the force by around 1pN, or $\sim$ 15% (inset). Note that, in the presence of phosphate, all measured forces were within the linear range.

2 Running the model

We compared our model to experimental measurements of bead displacement from small myosin ensembles in the laser trap, to measurements of actin filament speed in the motility assay and to measurements of force production and ATP consumption in muscle fibers. We modeled the small ensemble and motility assay experiments using stochastic (Monte-Carlo) simulations, and modeled many details of the experiments. We modeled the fiber experiments using a partial differential equation (PDE) model [e.g. 4, 5, 6] for the probability density of a given myosin molecule being in a particular state with a given molecular extension (sometimes called strain). We numerically solved these PDEs in steady-state. By using these PDE models, we neglect much of the complexity of the biological system, but we anticipate that our results will qualitatively match measurements. Here, we provide details of these simulations.

2.1 Monte-Carlo Simulations (laser trap and motility)

To perform Monte-Carlo simulations of a small myosin ensemble in the laser trap, we keep track of the state of every molecule, the extension of every actin-bound molecule, and the position of the actin filament. Our simulations are in one dimension. We assume that the actin filament is held by the laser trap, which behaves as a linear spring of stiffness k_{trap}. Each bound myosin is assumed to behave as a linear spring of stiffness k [3]. In the extremely viscous molecular environment, forces are balanced very quickly. We therefore assume that the force of the laser trap is balanced by the force of the bound myosin molecules. When a new myosin molecule binds to actin and undergoes its powerstroke or when a myosin molecule detaches from actin, the position of the filament (and, consequently, the extension of all bound myosin) is immediately changed to maintain force balance. The extension of a bound myosin determines the (average) force on that molecule, which then determines the ADP release rate, k_D.

We use the Gillespie Algorithm [7] to update the state of each myosin molecule in the ensemble as a function of time. Briefly, we calculate the time of every possible state transition in the model, picking values from

$$T_{ij} = -\frac{1}{k_{ij}} \ln(X) \tag{1}$$

where X is a uniformly distributed random variable between 0 and 1, and k_{ij} is the transition rate between state i and state j. We pick the minimum of these times, T_{min}, which corresponds to a particular state transition of a particular molecule, and we change the state of that molecule. We then increase time by T_{min}.

When myosin binds to actin, it may bind with non-zero extension. In particular, we choose an extension, x, from a Gaussian distribution with standard deviation (see [8])

$$\sigma_M = \sqrt{\frac{k_B T}{k}} \tag{2}$$

The position of the bead-actin-bead assembly also fluctuates. When myosin attaches, it "catches" the system in one position. Thus, we choose bead-actin-bead position from a Gaussian distribution with standard deviation

$$\sigma_A = \sqrt{\frac{k_B T}{k_{tot}}} \tag{3}$$

where k_{tot} is the sum of the stiffnesses of the laser trap k_{trap} and the overall stiffness of all attached myosin, kN_a where N_a is the number of attached myosin.

We simulate $\approx 10^4$ – 10^5 of chemical reactions to simulate a single experiment. The result of a simulation is the state of every molecule in the ensemble and the position of the bead-actin-bead assembly at the time of every molecular event, T_{ij}. To make the simulated position of the bead-actin-bead assembly consistent with our measurements, we perform a linear interpolation so that we have the position at 4kHz. At each of these times, we add some noise from a Gaussian distribution with standard deviation

$$\sigma_D = \sigma_A + \sigma_N \tag{4}$$

where $\sigma_N = 4$ nm is included to model background noise (e.g. electronic, vibrational, etc.). We analyzed these simulated data with the same algorithm as was used to analyze our experimental measurements. For our simulations, we used the parameters in Table 1. Those marked with an asterisk were determined from fits to data.

To model in vitro motility, we perform similar simulations, but ensemble size is fixed at 50 and attachment occurs at the rate k_a. At each time step, we require mechanical equilibrium, but there is no force applied on the filament by the laser trap, so that the forces of all attached myosin molecules balance. Simulations then give the position of actin as a function of time. To determine speed, we fit this position-time trace with a linear curve (ignoring the first 0.3 seconds, to eliminate non-steady state effects), and the slope of the best-fit line is our reported speed.

Parameter	Value	Parameter	Value
k_a^1	1s^{-1}	k	0.3 pN/nm
k_a	40s^{-1}	N	21^*
k_t	$2\mu\text{M}^{-1}\text{s}^{-1}$	k_a^2	1s^{-1*}
k_h^+	100s^{-1}	k_p	$30\text{mM}^{-1}\text{s}^{-1*}$
k_h^-	10s^{-1}	k_r^+	$0.7\text{mM}^{-1}\text{s}^{-1*}$
δ	-1.86nm	k_r^-	10s^{-1*}
k_d^0	350s^{-1}	k_{DP}	40s^{-1*}
d	10nm		

Table 1: Parameter values used in the model (see [9]). Starred entries are from fits to the present data (see sensitivity analysis).

2.2 Partial Differential Equation Simulations (muscle fibers, myofibrils)

To model force-velocity and isometric ATPase and force in fibers or myofibrils, we used a PDE model [4, 5, 6]. We have previously performed such PDE simulations for the model in the lack of phosphate [9]. The basic strategy of these models is to keep track of actin-bound and unbound states. For a given actin-bound state, i, we keep track of the probability density of being in that state with extension x at time t, $\eta_i(x,t)$. For a given unbound state, r, we keep track of the probability of being in that state at time t, $n_r(t)$. In general, these variables evolve according to equations of the form

$$\begin{aligned} \frac{\partial \eta_i}{\partial t} + v\frac{\partial \eta_i}{\partial x} &= \sum_j \left(k_{ji}(x)\eta_j - k_{ij}(x)\eta_i\right) + \sum_r \kappa_{ri}(x) n_r \\ \frac{dn_r}{dt} &= \sum_j \left(\int_{-\infty}^{\infty} k_{jr}(x)\eta_j dx\right) + \sum_i (n_i k_{ri} - n_r k_{ir}) \end{aligned} \tag{5}$$

where $\kappa_{ri}(x)$ is the rate density of transitioning from unbound state r to bound state i with extension x and $k_{ij}(x)$ is the rate of transitioning between bound state i to bound state j if the bound state has extension x. To these equations, there is also the constraint of total probability

$$\sum_j \int_{-\infty}^{\infty} \eta_j(x,t)dx + \sum_r n_r(t) = 1 \tag{6}$$

In steady-state, the equations become a set of coupled integro-ODEs. We numerically integrated them using a fourth-order Runge-Kutta method. At each step, we ensured that all integral constraints were satisfied using a standard root-find (the *fsolve* function in Matlab). At isometric steady-state, the equations further simplify into a set of integro-algebraic equations. These equations may be solved with a root find and matrix inversion.

3 Sensitivity analysis

The model has six unknown parameters that we must specify, $N, k_a^2, k_p, k_r^+, k_r^-, k_{DP}$. The Monte-Carlo simulations are relatively slow (a single function evaluation takes around a minute) and, being stochastic, have some inherent noise. As a result, determining the six parameters from a global fit to all the data is intractable. However, we can determine some parameters from a subset of the experiments, and then use these values in the remaining experiments. For example, we can estimate N and k_a^2 from laser trap data collected in the absence of phosphate.

3.1 Estimating N and k_a^2

To estimate model parameters N and k_a^2, we fit the data in the absence of phosphate. The parameter N is the ensemble size. The parameter k_a^2 accounts for the observation that a single molecule myosin binding

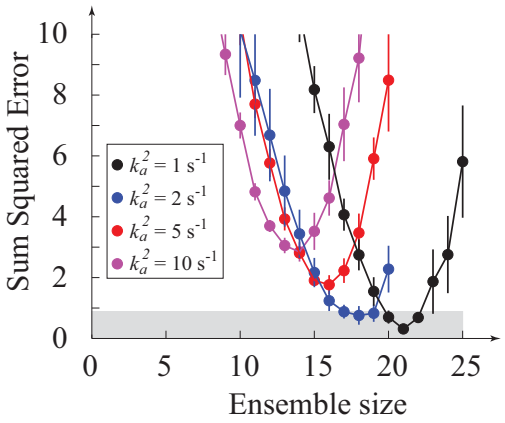

Figure 5: Sum of squared error as a function of ensemble size for several choices of attachment rate k_a^2. The best fit values are $k_a^2 = 1\text{s}^{-1}$ and $N = 21$. The shaded region gives an estimate of the fits within one standard deviation of the best-fit.

to actin in the laser trap is much slower than binding when myosin is part of a large ensemble [1]. This effect is likely to due to fluctuations in height of the actin filament above the myosin surface in the laser trap. As myosin molecules bind, they hold the filament near the surface, constraining its height, and thereby facilitating the binding of other myosin molecules. Thus, although a single molecule binds at $k_a^1 \approx 1\text{s}^{-1}$ [10], myosin binds to actin at $k_a \approx 40\text{s}^{-1}$ when part of a large ensemble (i.e. in the motility assay [9]). In between these two extremes, myosin should bind at an intermediate value, $k_a \leq k_a^2 \leq k_a^1$.

Our fitting criteria was the sum of the squared difference between the measured and simulated cumulative probability distributions of max event force and lifetime. To determine the optimum parameters, we evaluated the fit at ensemble sizes between 4 and 25 molecules, and attachment rates $k_a^2 = 1, 2, 5$ and 10s^{-1}. Since the simulations are stochastic, we evaluated the function five times to improve our estimates of the fit (see Fig. 5).

We find a best fit for $N = 21 \pm 3$ and $k_a^2 = 1 + 2$. We use these values in our simulations. For faster attachment, ensemble size can be smaller (i.e. for $k_a^2 = 2$, ensemble size can be as small as $N = 16$ and give a reasonable fit to the data).

3.2 Estimating k_{DP}

We can estimate k_{DP} from actin filament motility speed in the presence of high phosphate and ATP. Under these conditions, our experimental measurements suggest that nearly all of the flux goes through the phosphate-dependent branch of the kinetic model (see Fig. 1B of the main text). As a result, the expected attachment time $\langle t_{on} \rangle = 1/k_p[P]$. One nice feature of this situation is that all kinetic rates are entirely independent of force (since there is negligible flux through the "conventional" pathway, whereby actin-bound myosin releases ADP). The overall cycle time is then

$$\langle t_{cycle} \rangle \approx \frac{1}{k_p[P]} + \frac{1}{k_{DP}} + \frac{1}{k_h^+} + \frac{1}{k_a}$$

(note that, for simplicity, we neglect the reverse reaction k_h^-). The duty ratio, α, the proportion of total cycle time that myosin remains strongly bound to myosin, is

$$\alpha = \frac{\langle t_{on} \rangle}{\langle t_{cycle} \rangle} \approx \frac{1/k_p[P]}{\frac{1}{k_p[P]} + \frac{1}{k_{DP}} + \frac{1}{k_h^+} + \frac{1}{k_a}}$$

Unloaded speed in the motility assay, v, can be estimated from this value, the ensemble size (N_m) and the maximum actin velocity $V_{max} = d/k_p[P]$, where d is the power stroke size [11]. Thus

$$v = \frac{d}{k_p[P]} \left(1 - (1-\alpha)^{N_m}\right)$$

If duty ratio is small (as predicted by the model when phosphate concentration is high), we can approximate this speed as

$$v \approx \frac{d}{k_p[P]} \alpha N_m + O(\alpha^2)$$

Finally, if we take the limit of high phosphate, we get a simple expression

$$v \approx \lim_{[P]\to\infty} \frac{d}{k_p[P]} \alpha N_m = \frac{d N_m k_{DP} k_h^+ k_a}{k_h^+ k_a + k_{DP} k_a + k_{DP} k_h^+}$$

Given estimates of the values $v \approx 8000$ nm/s (motility at saturating ATP), $d = 10$ nm, $k_a = 40\text{s}^{-1}$ and $k_h^+ = 100\text{s}^{-1}$, $N_m = 50$, we have

$$k_{DP} = \frac{6400}{176}\text{s}^{-1} = 36\text{s}^{-1}$$

Based on this calculation, we use $k_{DP} = 40\text{s}^{-1}$ in our simulations.

3.3 Estimating k_{off}, k_r^+, k_r^-

We determined the remaining three parameters, k_{off}, k_r^+, k_r^- from optimization of fit. We measured goodness of fit by the sum of the squared difference between the measured and simulated cumulative probability distributions of max event force and lifetime for each of the three phosphate concentrations (5, 10 and 30 mM, see Fig. 6A–D, upper right insets). We normalized this value by dividing by the best fit value at $k_{off} = 30\text{s}^{-1}\text{mM}^{-1}$. To this value, we added the χ^2 value from fits to motility in the presence of 30mM phosphate (data from [12], see Fig. 6A–D, lower right insets), normalized by dividing by the best fit χ^2 value at $k_{off} = 30\text{s}^{-1}\text{mM}^{-1}$. Since the simulations are stochastic, we evaluated the goodness-of-fit ten times to improve our estimates.

We evaluated $k_{off} = 20, 30, 60$ and $120\text{s}^{-1}\text{mM}^{-1}$. At each of these values, we varied k_r^+ and k_r^- to determine the best fit. The fits are shown in Fig. 6A–D.

At $k_{off} = 20\text{s}^{-1}\text{mM}^{-1}$, the model could not fit the data. In particular, the model was unable to reproduce the laser trap measurements (see Fig. 6E and Fig. 6A). For all other values of k_{off} we investigated (30, 60 and 120 $\text{s}^{-1}\text{mM}^{-1}$), the model could fit the laser trap data and simultaneously fit the in vitro motility data of [12]. The best fit was $k_{off} = 60\text{s}^{-1}\text{mM}^{-1}$ (see Fig. 6E). At each value of k_{off}, goodness-of-fit depended sensitively on the ratio k_r^-/k_r^+, and was less sensitive to their precise values.

The model was able to fit the data for a wide range of k_{off} (30-$120\text{s}^{-1}\text{mM}^{-1}$). This wide range is likely due to the very strong effect of phosphate on these small ensembles. Thus, there is a large decrease in event force and lifetime from 0 to 5 mM phosphate, but a much more subtle decrease in these values as phosphate is increased further (i.e. to 10 or 30 mM, see Fig. 2 of the main text). The sensitivity analysis allows us to put a lower-bound on k_{off} ($k_{off} > 20\text{s}^{-1}\text{mM}^{-1}$), but does not let us clearly determine an upper bound. We performed additional experiments to help refine our parameter estimates.

According to the model, phosphate has a strong effect on these small ensembles because it lowers the duty ratio. Thus, in the absence of phosphate, several myosin often interact with actin to generate short runs of motility. However, in the presence of even 5mM phosphate, these runs of motility are much less prevalent (see the section "More detailed comparisons between model and experiment" for more details). We therefore re-did our measurements at a higher myosin density (40 μg/mL, a 1.6-fold increase). Under these conditions, we expect that runs of motility will occur in the presence of phosphate, allowing us to more precisely determine an upper bound on k_{off}.

We fit these data with the best-fit parameters for $k_{off} = 60\text{s}^{-1}\text{mM}^{-1}$ ($k_r^+ = 7\text{s}^{-1}\text{mM}^{-1}$ and $k_r^- = 45.5\text{s}^{-1}$) and $k_{off} = 30\text{s}^{-1}\text{mM}^{-1}$ ($k_r^+ = 0.7\text{s}^{-1}\text{mM}^{-1}$ and $k_r^- = 10\text{s}^{-1}$) allowing ensemble size to vary between 1 and 40. The fits for $k_{off} = 30\text{s}^{-1}\text{mM}^{-1}$ are shown in Fig. 7A. As expected, these data allow us to more sensitively characterize the number of myosin at 5 and 10 mM P_i (observe the more parabolic shape of the curves at 40 μg/mL in Fig. 7A). We also find that, at the lower myosin density (25μg/mL) $k_{off} = 60\text{s}^{-1}\text{mM}^{-1}$ fit the trap data nearly as well as $k_{off} = 30\text{s}^{-1}\text{mM}^{-1}$. But, at the higher myosin density (40μg/mL) the fit for $k_{off} = 60\text{s}^{-1}\text{mM}^{-1}$ was significantly worse than the fit for $k_{off} = 30\text{s}^{-1}\text{mM}^{-1}$ (see Fig. 7B). We therefore estimate that $k_{off} = 30\text{s}^{-1}\text{mM}^{-1}$, $k_r^+ = 0.7\text{s}^{-1}\text{mM}^{-1}$ and $k_r^- = 10\text{s}^{-1}$. We used these values in our simulations.

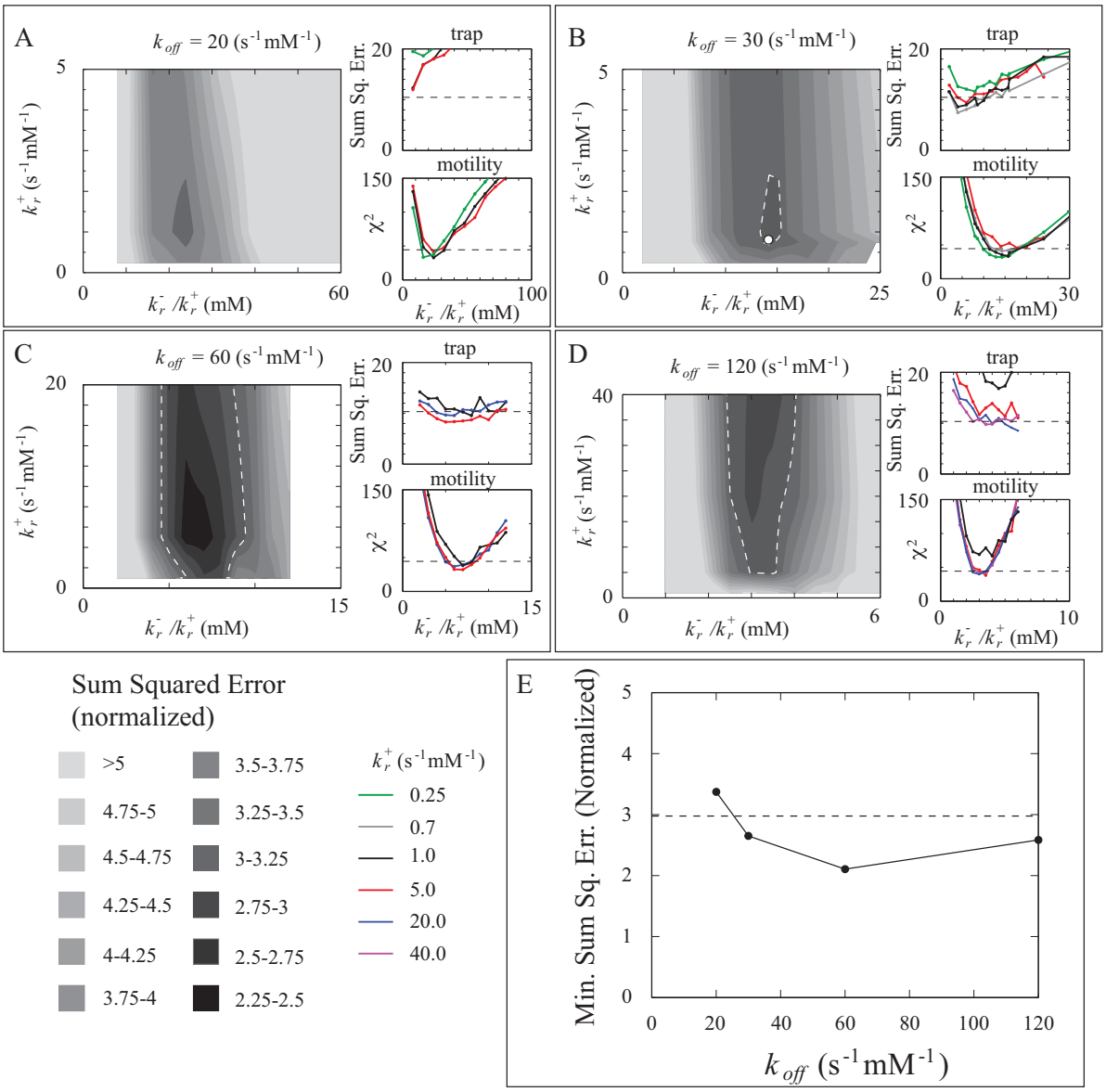

Figure 6: Sensitivity analysis of parameter estimates for k_{off}, k_r^+ and k_r^-. A–D show a two dimensional plot of normalized sum squared error as a function of k_r^+ and k_r^-/k_r^+ for $k_{off} = 20, 30, 60$ and $120 \text{s}^{-1}\text{mM}^{-1}$, respectively. The white dashed line indicates the parameter combinations that can adequately fit the data. The hollow dot indicates our best guess of parameter values. Line and contour colors are defined in the legend at lower right. The inset shows the sum of the squared error for the trap data (top) and χ^2 value for the motility data of [12] (bottom). The χ^2 value is likely too high because of an under-reporting of experimental error at low motility speeds. The dashed line indicates one standard deviation from the best-fit values. E. Minimum error as a function of k_{off}. The dashed line indicates the allowable range of k_{off}. Of the four values we investigated, we can only rule out $k_{off} = 20 \text{s}^{-1}\text{mM}^{-1}$.

These fits also allowed us to refine our estimate of ensemble size. Except for data collected in the absence of phosphate, the model predicts a smaller number of myosin molecules at 25 μg/mL than at 40 μg/mL (see Fig. 7C). From these data, we estimate an ensemble size of $N \approx 16$ at 25 μg/mL and $N \approx 24$ at 40 μg/mL. In the absence of phosphate, the model predicts that average ensemble size actually decreases at the higher myosin density. This result is likely due to the fact that large ensembles are expected to generate sufficiently large forces to overpower the trap and are therefore not included. Thus, the ensemble size measured in the

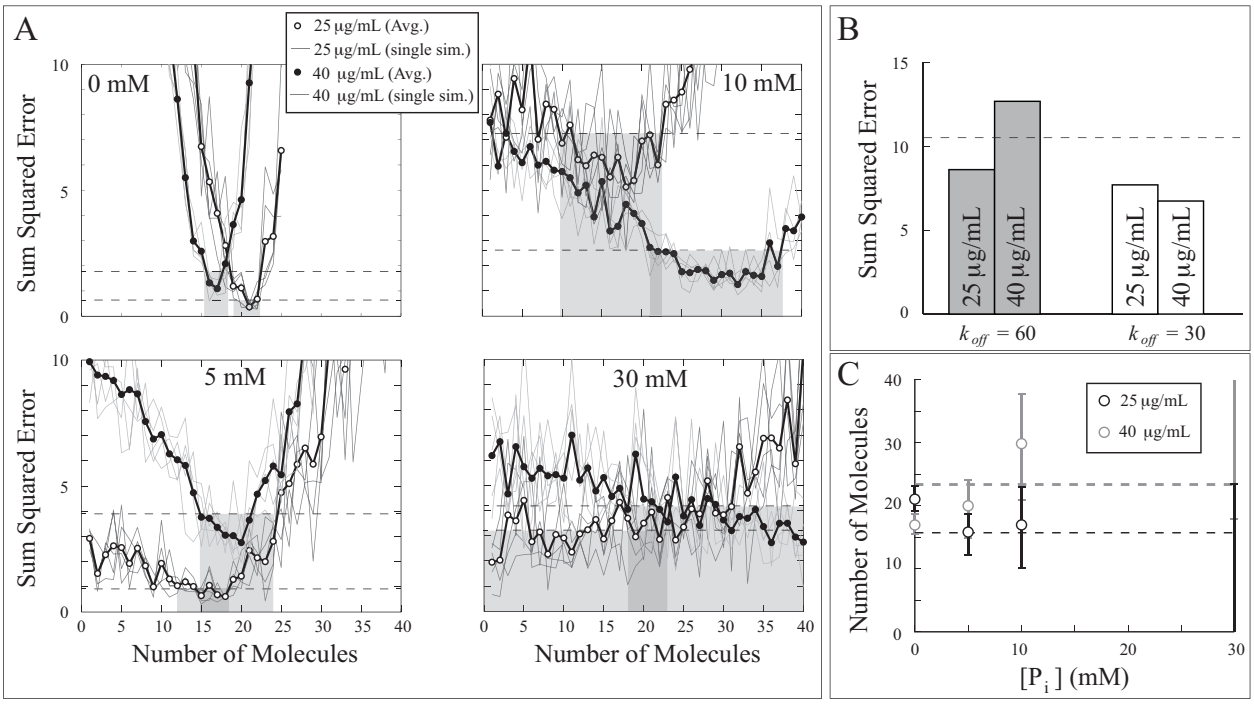

Figure 7: Fits with $k_{off} = 30\text{s}^{-1}\text{mM}^{-1}$ fit laser trap measurements at high myosin density (40 μg/mL) significantly better than fits with $k_{off} = 60\text{s}^{-1}\text{mM}^{-1}$. A. Estimating ensemble size and goodness-of-fit for $k_{off} = 30$. Dashed lines indicate the sum of the squared error that is approximately one standard deviation from best fit. Shaded regions indicate the associated ranges in ensemble size N. B. Best fits to the data for $k_{off} = 60$ (left, shaded) and $k_{off} = 30$ (right, unshaded). The dashed line indicates one standard deviation from best fit. C. Ensemble size estimates for $k_{off} = 30$, the hollow dots represent the best fit value. The error bars indicate the standard deviation (the shaded region in part A). Note that, for 30 mM P_i, the best fit values are missing, since neither curve had a clear minimum.

absence of phosphate likely reflects the maximum ensemble that the measurement system can support under these conditions.

4 More detailed comparisons between model and measurements

We measured binding event lifetime and maximum force at four different phosphate concentrations (0, 5, 10 and 30mM) at two different myosin densities (25 and 40μg/mL). We fit the distributions of event lifetime and event maximum force, but these fits neglect the correlation between lifetime and force (one would expect that, in general, longer events should have higher force). We therefore compared simulated and measured two dimensional histograms of event force and lifetime (see Fig. 8). The model is consistent with our measurements, recapitulating many features of the data.

We looked in more detail at whether the model could replicate specific aspects of the data. In particular, we compared the number of high force events ($F > 1.5$pN) as a function of phosphate concentration at both myosin densities (25 and 40μg/mL, see Fig. 9A). The model is broadly consistent with the data, but slightly underestimates the proportion of high force events at 40μg/mL. We also compared the number of negative force events ($F < 0$pN) as a function of phosphate concentration at both myosin densities (25 and 40μg/mL, see Fig. 9B). Again, the model is broadly consistent with the data. Note that in the model these negative force events occur, not because of the reversal of the powerstroke, but rather due to Brownian capture of actin. Finally, we compared the number of long lifetime events ($T > 200$ms) as a function of phosphate concentration at both myosin densities (25 and 40μg/mL, see Fig. 9C). The model agrees with the data. Thus, we conclude that the model faithfully reproduces, not only average force and lifetime (see Fig. 2 of

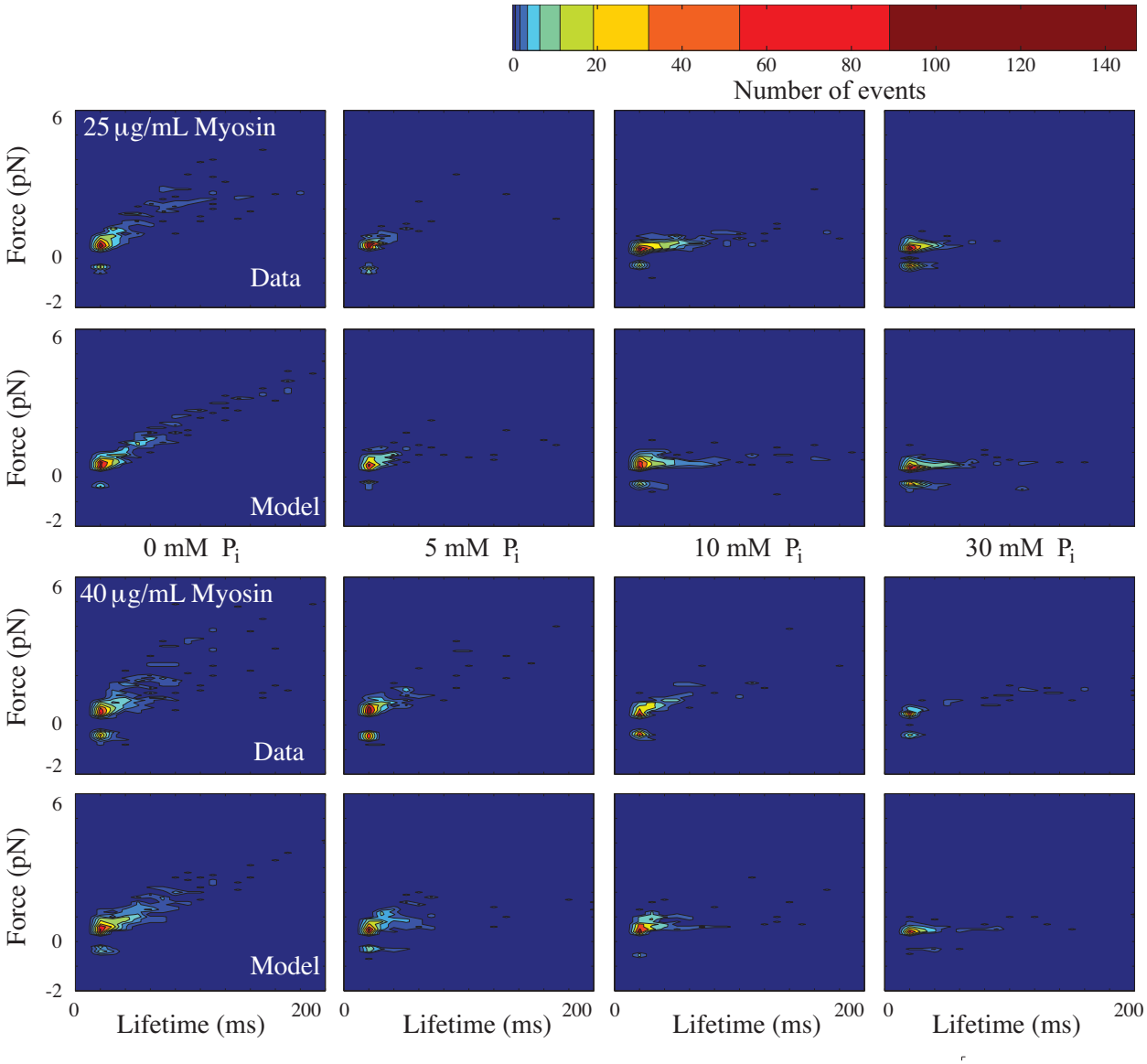

Figure 8: Two dimensional histograms of event lifetime and maximum force from small myosin ensembles in the laser trap. Top and second row show measurements and simulations, respectively, at a myosin density of 25 μg/mL. Third and bottom row show measurements and simulations, respectively, at a myosin density of 40 μg/mL. Phosphate concentration increases from left to right.

the main text), but also many aspects of the distribution of event forces and lifetimes.

Although it replicates aspects of the distributions of event forces and lifetimes, our model (like all models) can only approximate reality. We assume, for example, that all measurements were from ensembles containing precisely 21 independent myosin heads. In reality, each data set consisted of measurements from 15-20 myosin coated pedestals, each of which likely had a slightly different number of available myosin heads. To determine whether these approximations affect the ability of the model to fit our measurements, we performed a more detailed comparison between modeled and measured maximum event forces in the absence of phosphate (see Fig. 10).

We ran 20 simulated experiments with an identical number of binding events as in the measurement. The cumulative probability distribution of these 20 simulations, along with our measurement, is shown in Fig. 10A. For the most part, the agreement between the simulations and the measurement is good. However,

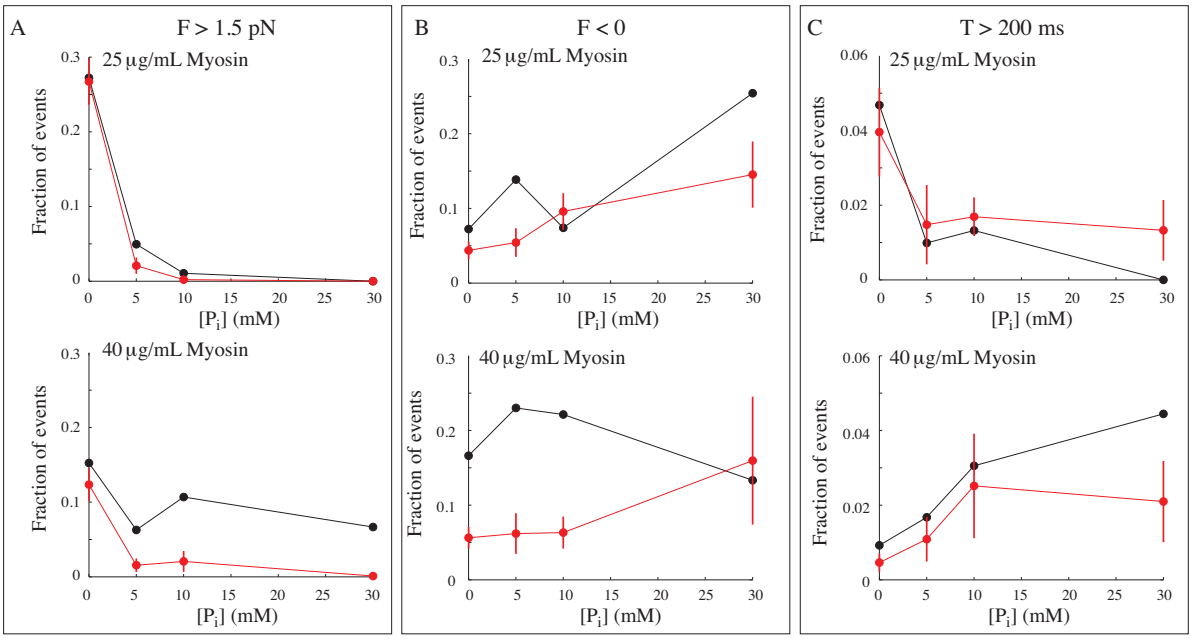

Figure 9: Simulated and measured distributions of event forces and lifetimes share many qualities besides average values. In all plots, measurements are shown in black and the model in red. Error bars on the model are standard deviations of 10 simulations. Top shows simulations and measurements at 25 μg/mL (simulations at $N = 21$ for all phosphate concentrations); bottom shows simulations and measurements at 40 μg/mL (simulations at $N = 17, 21, 30$ and 30 for phosphate concentrations of 0, 5 10 and 30 mM, respectively). A. Shows the proportion of high force events (events with maximum forces greater than 1.5 pN) as a function of phosphate concentration. B. Shows the proportion of negative force events (events with maximum forces less than 0 pN) as a function of phosphate concentration. Note that the model does not include powerstroke reversal, so these negative force events are due to myosin's Brownian capture of the actin filament. C. Shows the proportion of long lifetime events (events with lifetimes greater than 200 ms).

there are three points (indicated with gray arrows) where the model slightly under-predicts the probability density. These three points are also apparent in the histogram (Fig. 10B), where the model under-predicts the number of events. In all cases, however, this error is small (less than 10 events, see Fig. 10B, inset), suggesting that the model is able to replicate most aspects of the experimental measurement. Being small, the exact source of this error is difficult to pinpoint.

5 Model predictions of phosphate's effect

Here, we suppose that the model faithfully represents most aspects of myosin's interaction with actin under the conditions of our experimental measurements. We may then answer questions that are difficult to measure experimentally. For example, in our experiments, how many myosin molecules are bound? How is myosin's duty ratio affected by phosphate? What is the flux through the two different pathways of our model in each experimental condition? How important is phosphate's binding to the rigor state? We now address each of these questions in turn.

We determined the number of myosin molecules that are bound to actin in our laser trap experiments at a myosin density of 25μg/mL. More specifically, we determined the proportion of time that 1, 2, 3, etc. myosin molecules were bound in our simulations. Under all conditions, single molecule attachments were the most common, accounting for $59\%, 77\%, 88\%$ and 93% of the time that at least one myosin was bound to actin at $0, 5, 10$ and 30mM P_i, respectively. As expected from our measurements, single molecule attachments become more prevalent at high phosphate concentrations and, conversely, multiple molecule attachments are virtually eliminated at 30 mM phosphate (see Fig. 11A).

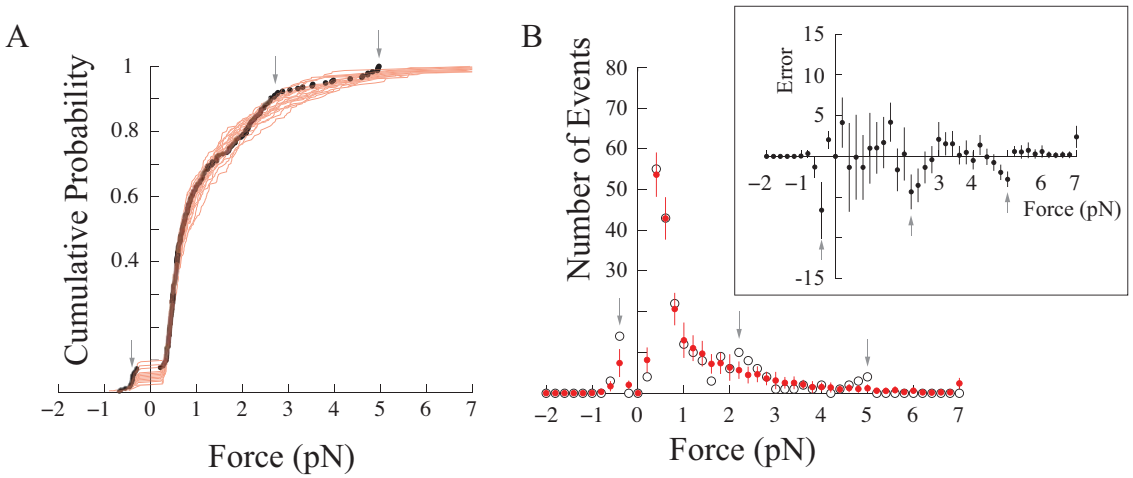

Figure 10: Good agreement between simulated and measured cumulative probability distribution and histograms of maximum force in the absence of phosphate. In all plots, there are three places (indicated with gray arrows) where the model under-predicts the number of events. The model is shown in red, the measurement in black. A. Cumulative probability as a function of force. B. A histogram of the same data, error bars are standard deviation. Inset shows the difference between the simulation and measurement (error bars are standard deviation).

Under the experimental conditions examined here (an ATP concentration of 100 μM and isolated myosin adhered to a coverslip) the model predicts that myosin's duty ratio decreases in the presence of phosphate, due to phosphate-induced detachment. It is important to note that myosin's attachment rate, and therefore duty ratio, depends on the number of myosin molecules bound to the actin filament (typically being around 1 s^{-1} for a single molecule, but increasing to around 40 s^{-1} under conditions where many myosin are bound to actin, as in the motility assay). We therefore examined how phosphate affects myosin's duty ratio in the in simulations of the in vitro motility assay. Simulations show that duty ratio decreases from ≈ 0.2 in the absence of phosphate to ≈ 0.05 at 30 mM phosphate – roughly a four-fold decrease (see Fig. 11B).

Using the model, we can determine the probability that myosin goes through the "conventional" pathway (the green pathway in Fig. 1B of the main text), releasing ADP while strongly bound to actin and binding ATP prior to detachment, P_c. Then, the probability that myosin goes through the phosphate dependent branch (the red pathway in Fig. 1B of the main text) is $P_p = 1 - P_c$. We determined P_c for the simulated small ensemble laser trap experiments by counting the number of times the molecules went through the conventional pathway, n_c, and the number of times the molecules went through the phosphate-dependent pathway, n_p. Then, $P_c = n_c/(n_p + n_c)$. The results are shown in Fig. 11C for the simulated experiments at 25μg/mL myosin. Naturally, in the absence of phosphate, all myosin molecules go through the conventional pathway $P_c = 1$. This value decreases to $P_c = 0.23$ at 30 mM phosphate, meaning that 77% of the molecules release ADP off actin (in the phosphate-dependent pathway) under these conditions (see Fig. 11C). For these simulations, we can approximate P_c by neglecting force dependence and writing

$$P_c = \frac{k_D}{k_D + k_{off}[P]} \approx \frac{k_d^0}{k_d^0 + k_{off}[P]}$$

This approximation works because, at the phosphate concentrations and ensemble sizes considered here, most binding events only involve a single myosin molecule (see Fig. 11A) so myosin experiences negligible force. The approximation is less successful in the motility assay, where intermolecular forces are more important (see [9]).

The model includes phosphate binding to actin-bound myosin after the myosin has released both phosphate and ADP (i.e. while it is in the rigor state). In our model, rigor binding is necessary to fit the data (see Sensitivity Analysis). Such rigor binding can explain the inhibitory effect of phosphate on motility speed at low ATP concentrations [12, 13]. It is unclear, however, how important this state is at higher ATP concentrations. We performed simulations in order to try to measure the importance of this state.

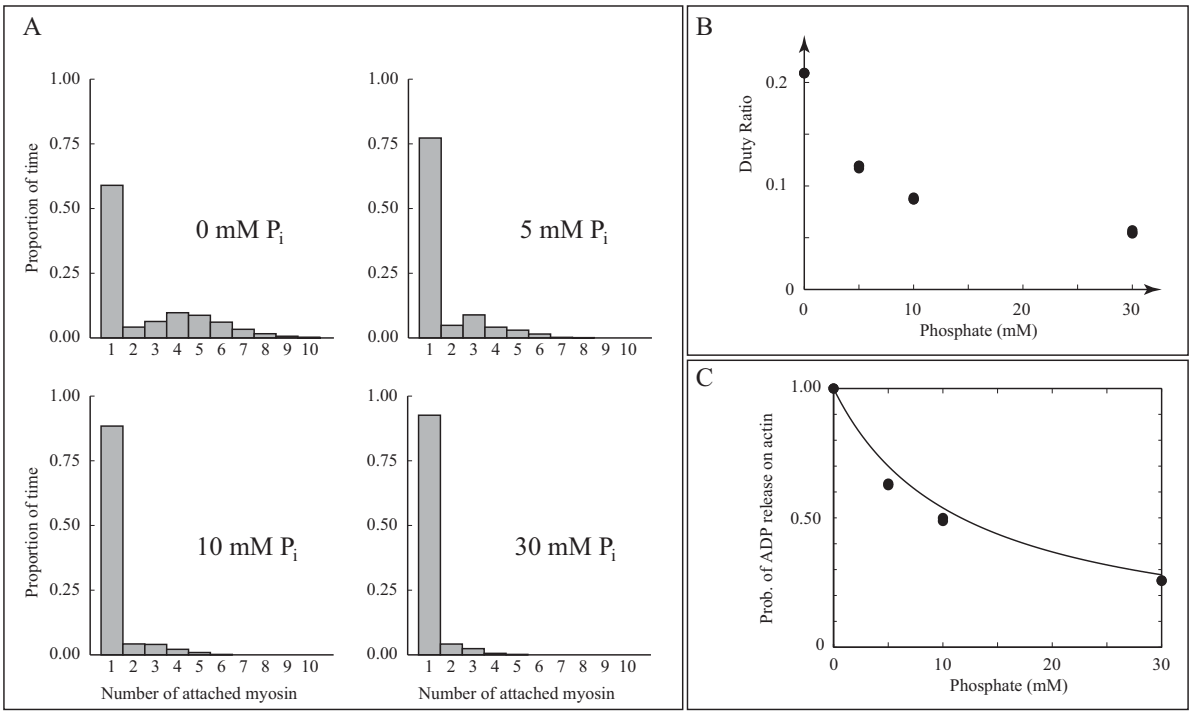

Figure 11: Using the model to predict various aspects of phosphate's effect on myosin's interaction with actin. A. Predicting the number of myosin molecules interacting with actin at different phosphate concentrations. See text for experimental conditions used in the simulations. B. Predicting duty ratio as a function of phosphate. The calculations were performed for a large ensemble of myosin and 100 μM ATP. Different experimental conditions would likely give a different relationship. C. Predicting the probability of going through the "conventional" pathway, whereby ADP is released on actin. As phosphate increases, the model predicts that phosphate increasingly induces detachment from actin and ADP is then released off actin.

One measure of the importance of a state is the probability of a molecule entering that state, P_R. Since none of the kinetic steps are force-dependent in the model, we can precisely calculate this value

$$P_R = \frac{k_r^+[P]}{k_t[T] + k_r^+[P]}$$

where $[T]$ is the concentration of ATP and $[P]$ is the concentration of phosphate. Even at high phosphate concentrations, the probability of forming the AM.P$_i$ state is small ($P_R < 0.1$) for ATP concentrations of 100μM or greater (see Fig. 12A). Note that physiological ATP concentrations are around 1-5 mM. Thus, one might naively conclude that this state is not very important.

A different set of simulations, however, suggest that the state is important, even at physiological ATP concentrations. First, we simulated our experimental measurements of binding event lifetime without the AM.P$_i$ state (by setting $k_r^+ = 0$) and compared the results to simulations with the AM.P$_i$ state (where the best-fit value was $k_r^+ = 0.7\text{mM}^{-1}\text{s}^{-1}$). Rigor binding had a dramatic effect on the average event lifetime (see Fig. 12B), more than doubling it at a phosphate concentration of 30 mM. Second, we simulated in vitro motility both without ($k_r^+ = 0$) and with ($k_r^+ = 0.7\text{mM}^{-1}\text{s}^{-1}$). Even for ATP concentrations of 1mM, there was a strong difference (see Fig. 12C), with rigor binding decreasing motility speed from 6.4 μm/s to 4.7 μm/s, a reduction of about 30%. Thus, even though the AM.P$_i$ state occurs only rarely, it has a large effect when it does.

We can understand this apparent discrepancy by noting that phosphate unbinds from the AM.P$_i$ state rather slowly, at $k_r^- = 10\text{s}^{-1}$. Thus, on average, this state lasts for $1/k_r^- = 100$ms. At high ATP concentrations where binding lifetime is much shorter than 100ms, even though this state is rarely formed, it has a large effect when it does form. For example, at 1mM ATP if the AM.P$_i$ state is not formed, strong

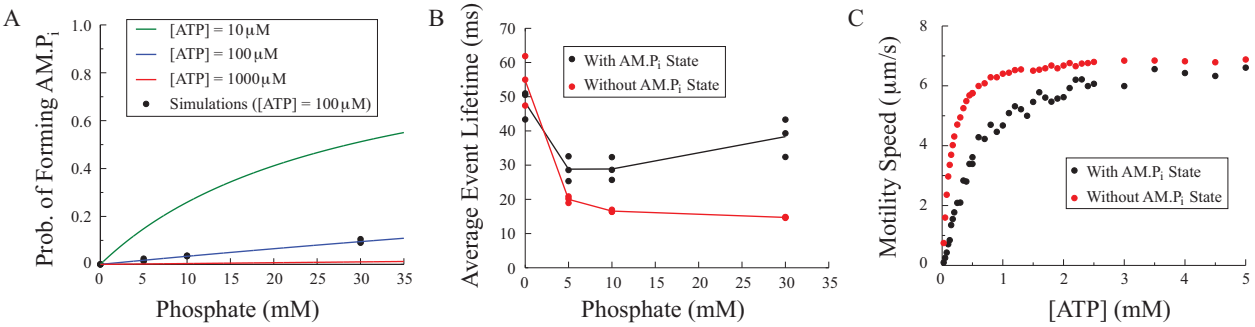

Figure 12: Phosphate binding to the rigor state is important, even at physiological ATP concentrations. A. The probability of phosphate binding to the rigor state and forming the AM.P$_i$ state, which is very small at high ATP. Naively one might conclude that formation of AM.P$_i$ state is not important at high ATP. B. Even though the AM.P$_i$ state is rarely formed, it has a large effect on average event lifetime in our simulated measurements at 100 μM ATP. C. According to the model, formation of the AM.P$_i$ state has a measurable effect on motility speed, even at physiological (mM) ATP concentrations. The AM.P$_i$ state has an effect because, even though it is rarely formed, it has a large effect when it does.

binding lasts $1/kt[T] + 1/k_D \approx 3.5$ms. Alternatively, when the AM.P$_i$ state is formed, strong binding lasts $1/kt[T] + 1/k_D + 1/k_r^- \approx 103.5$ms – a 30-fold increase. This drastic increase in attachment lifetime means that, even though the AM.P$_i$ is formed only $\sim 1\%$ of the time, it still has a measurable effect (see Fig. 12C).

References

[1] Baker, J. E., C. Brosseau, P. B. Joel, and D. M. Warshaw. 2002. The biochemical kinetics underlying actin movement generated by one and many skeletal muscle myosin molecules. Biophys. J. 82: 2134-2147 PM:11916869.

[2] Guilford, W. H., D. E. Dupuis, G. Kennedy, J. Wu, J. B. Patlak, and D. M. Warshaw. 1997. Smooth muscle and skeletal muscle myosins produce similar unitary forces and displacements in the laser trap. Biophys. J. 72: 1006-1021 PM:9138552.

[3] Veigel, C., M. L. Bartoo, D. C. White, J. C. Sparrow, and J. E. Molloy. 1998. The stiffness of rabbit skeletal actomyosin cross-bridges determined with an optical tweezers transducer. Biophys. J. 75: 1424-1438 PM:9726944.

[4] Huxley, A. F. 1957. Muscle structure and theories of contraction. Prog. Biophys. Biophys. Chem., 7:255–318.

[5] Lacker, H. M., 1977. Cross-bridge dynamics in skeletal muscle: mathematical methods for determining the reaction rate and force-extension curves of cross-bridges from the macroscopic behavior of muscle. PhD diss., NYU.

[6] Lacker, H. M. and C. S. Peskin. 1986. A mathematical method for the unique determination of cross-bridge properties from steady-state mechanical and energetic experiments on macroscopic muscle. Lect. Math Life Sci., 16:121–153.

[7] Gillespie, D. T. 1977. Exact Stochastic Simulation of Coupled Chemical Reactions. J. Phys. Chem. 81: 2340-2361.

[8] Srinivasan, M. and S. Walcott. 2009. Binding site models of friction due to the formation and rupture of bonds: state-function formalism, force-velocity relations, response to slip velocity transients, and slip stability. Phys. Rev. E, 80(4), 046124.

[9] Walcott, S., D. M. Warshaw, and E. P. Debold. 2012. Mechanical coupling between myosin molecules causes differences between ensemble and single-molecule measurements. Biophys. J., 103:501–510.

[10] Kad, N. M., S. Kim, D. M. Warshaw, ., VanBuren, and J. Baker. 2005. Single-myosin crossbridge interactions with actin filaments regulated by troponin-tropomyosin. Proc. Natl. Acad. of Sci., 102(47), 16990-16995.

[11] Uyeda, T. Q., S. J. Kron and J. A. Spudich (1990). Myosin step size: estimation from slow sliding movement of actin over low densities of heavy meromyosin. J. Mol. Biol., 214(3), 699-710.

[12] Debold, E. P., M. A. Turner, J. C. Stout, S. Walcott. 2011. Phosphate enhances myosin-powered actin filament velocity under acidic conditions in a motility assay. Am. J. Physiol Regul. Integr. Comp Physiol 300: R1401-R1408.
[13] Amrute-Nayak, M., M. Antognozzi, ..., B. Brenner. 2008. Inorganic phosphate binds to the empty nucleotide binding pocket of conventional myosin II. J. Biol. Chem. 283: 3773-3781.